Growth mechanism and domain structure study on epitaxial $BiFeO_3$ film grown on $(La_{0.3}Sr_{0.7})(Al_{0.65}Ta_{0.35})O_3$

In-Tae Bae (iD), Shintaro Yasui (iD), Tomohiro Ichinose (iD), Mitsuru Itoh (iD), Takahisa Shiraishi (iD), Takanori Kiguchi (iD), and Hiroshi Naganuma (iD)

View Online   Export Citation   CrossMark

ARTICLES YOU MAY BE INTERESTED IN

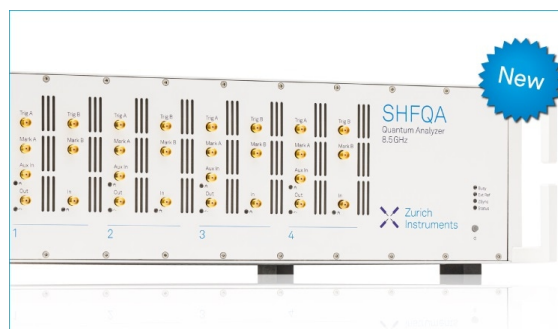In-plane ferroelectricity and enhanced Curie temperature in perovskite $BaTiO_3$ epitaxial thin films
Applied Physics Letters **117**, 072902 (2020); https://doi.org/10.1063/5.0013484

A magnetic phase diagram for nanoscale epitaxial $BiFeO_3$ films
Applied Physics Reviews **6**, 041404 (2019); https://doi.org/10.1063/1.5113530

Structural investigation of ferroelectric $BiFeO_3$–$BaTiO_3$ solid solutions near the rhombohedral–pseudocubic phase boundary
Applied Physics Letters **116**, 252902 (2020); https://doi.org/10.1063/5.0008990

Growth mechanism and domain structure study on epitaxial BiFeO₃ film grown on (La$_{0.3}$Sr$_{0.7}$)(Al$_{0.65}$Ta$_{0.35}$)O₃

In-Tae Bae,[1,2,a)] (ID) Shintaro Yasui,[3,4,a)] (ID) Tomohiro Ichinose,[5] (ID) Mitsuru Itoh,[3] (ID) Takahisa Shiraishi,[6] (ID) Takanori Kiguchi,[6] (ID) and Hiroshi Naganuma[5,7,8,9] (ID)

AFFILIATIONS

[1]Small Scale Systems Integration and Packaging Center, State University of New York at Binghamton, Binghamton, New York 13902, USA
[2]Department of Physics, State University of New York at Binghamton, Binghamton, New York 13902, USA
[3]Laboratory for Materials and Structures, Tokyo Institute of Technology, 4259-J2-19, Nagatsuta-cho, Midori-ku, Yokohama 226-8503, Japan
[4]Laboratory for Advanced Nuclear Energy, Tokyo Institute of Technology, 2-12-1, Ookayama, Meguro-ku, Tokyo 152-8550, Japan
[5]Department of Applied Physics, Graduate School of Engineering, Tohoku University, Sendai 980-8579, Japan
[6]Institute for Materials Research, Tohoku University, Sendai, Japan
[7]Center for Innovative Integrated Electronic System (CIES), Tohoku University, 468-1, Aoba, Aramaki, Aoba-ku, Sendai 980-8572, Japan
[8]Center for Spintronics Research Network (CSRN), Tohoku University, 2-1-1, Katahira, Aoba-ku, Sendai 980-8577, Japan
[9]Center for Science and Innovation in Spintronics (CSIS), Tohoku University, 2-1-1, Katahira, Aoba-ku, Sendai 980-8577, Japan

[a)]**Authors to whom correspondence should be addressed:** itbae@binghamton.edu and yasui.s.aa@m.titech.ac.jp

ABSTRACT

A BiFeO₃ (BFO) film is epitaxially grown on an (La$_{0.3}$Sr$_{0.7}$)(Al$_{0.65}$Ta$_{0.35}$)O₃ (LSAT) substrate to investigate the lattice mismatch effect on the domain structure and lattice strain status within the BFO film. Atomic resolution scanning transmission electron microscope image, selected area electron diffraction (SAED) patterns, and X-ray reciprocal space mapping (XRSM) data clearly reveal that the lattice strain originating from the lattice mismatch between BFO and LSAT is relaxed by causing misfit dislocations in the BFO film. The SAED and XRSM data indicate that the crystal structure of BFO film is rhombohedral with the space group *R3c*. In particular, XRSM data acquired along two different in-plane orientations reveal that the BFO layer consists of two different domains that were 90° off each other with respect to the surface normal orientation. An atomistic model based on the crystal orientation relation found by SAED and XRSM shows that (1) the ferroelectric polarization axes of both domains are 35.6° with respect to the BFO film surface and (2) the two domains are consistent with the so-called 71° (and/or 109°) ferroelectric domains reported previously. The lattice mismatch of ~2.8% calculated based on the epitaxial relation is proposed to be too large to be stored as elastic strain energy within the BFO layer.

Published under license by AIP Publishing. https://doi.org/10.1063/5.0005672

INTRODUCTION

BiFeO₃ (BFO) is by far the most widely studied multiferroic material because its unique property, i.e., the combination of large ferroelectric polarization ($\sim100\,\mu C\,cm^{-2}$) and *G*-type antiferromagnetism well above room temperature, implies tremendous potential in spintronics and smart energy applications.[1–3] It may be worth noting that there had been a debate over whether $\sim100\,\mu C\,cm^{-2}$ of

ferroelectric polarization value reported for an epitaxially grown BFO film is an enhanced value caused by lattice mismatch or is the intrinsic value for unstrained BFO material.[4] Subsequent discovery of the same ferroelectric polarization value in high-quality bulk BFO confirms that $\sim100\,\mu C\,cm^{-2}$ is the intrinsic value of unstrained BFO material.[5,6] In fact, an *ab initio* calculation also proves that the ferroelectric polarization value of BFO is

intrinsically high, i.e., 90–100 μC cm^{-2}.[7] Nonetheless, epitaxial growth of BFO using a variety of single crystal substrates has been investigated in an attempt to understand and/or enhance its physical property by imparting the lattice strain caused by lattice misfit with the substrate materials.[8] Since the physical properties such as ferroelectric polarization and magnetism are strongly related to the crystalline structure and atomic bonding nature, extensive structural study works have been performed over the last couple of decades. As a result, it has been found experimentally that atomistic bonding in epitaxial BFO is sufficiently *flexible* to adapt with the lattice mismatch caused by the substrate material to form a variety of crystal symmetries other than its equilibrium rhombohedral symmetry, i.e., space group *R3c*.[9–20] The strain effect on the BFO structure was studied theoretically as well by investigating the possibility of more than a few metastable BFO phases depending on the amount of lattice strain applied.[9,16,21] However, the details about strain effect on the BFO crystal structure as well as the evaluation of lattice strain remain a challenging task primarily due to the highly complex structural nature within BFO.[22,23]

Conventionally, pseudocubic notation has been used to describe the crystal symmetry found within epitaxially grown BFO because of its convenience over hexagonal notation that describes rhombohedral symmetry impeccably. As a result, the discussion about crystal structure within epitaxial BFO is mostly about the symmetry in crystal unit cell vectors. This means another important factor in terms of crystal symmetry evaluation, i.e., *basis atom locations* within the unit cell, is disregarded. In order to address this issue, our group has suggested a novel methodology that combines (1) X-ray diffraction (XRD) for the accurate evaluation of crystal unit cell vectors and (2) transmission electron microscopy (TEM) with structure factor calculation to investigate the basis atom location effect on the symmetry. This method has proved highly effective for identifying the correct space group of *Cm*, i.e., monoclinic, found in highly strained BFO.[20] This is remarkable because the basis atoms' location of the unit cell decreases the symmetry of the BFO from orthorhombic to monoclinic.[20]

Single crystalline $(La_{0.3}Sr_{0.7})(Al_{0.65}Ta_{0.35})O_3$ (LSAT) substrates were originally fabricated for epitaxial growth of superconductor films because they overcome technical difficulties that the LaAlO$_3$ substrate has, such as twinning, lattice strain, and non-isotropic properties.[24] Later, LSAT turns out useful for microwave application owing to its low-dielectric loss and medium dielectric constant.[25] Besides, the cost becomes comparable to that of SrTiO$_3$. Thus, LSAT became increasingly popular as a substrate in a variety of thin film epitaxy.

In this study, we investigate the effect of the $(La_{0.3}Sr_{0.7})(Al_{0.65}Ta_{0.35})O_3$ substrate on BFO epitaxial growth in terms of (1) how lattice strain affects crystal and domain structures, (2) quantitative lattice mismatch evaluation based on epitaxial relation analysis, and (3) the possible configurations of the ferroelectric polarization orientations in domains.

EXPERIMENTAL PROCEDURE

An epitaxial BFO film (8×8 mm^2) was grown on an (100) LSAT substrate (10×10 mm^2) by using the ultrahigh vacuum ($<2 \times 10^{-6s}$ Pa) radio frequency (rf) sputtering technique manufactured by ULVAC Inc., Japan, at a growth temperature of 550 °C. A

mixture of Ar and O$_2$ gases was used with the O$_2$ flow varying by 1.8%–14.5% under a fixed pressure of 0.4 Pa. A sintered BFO target from Toshima Manufacturing, Japan, was used as the sputtering target. Upon completion of the BFO film deposition, the sample was allowed to cool down to room temperature under the vacuum naturally. Note that the growth temperature used here is substantially lower than the typical growth temperature of ~700 °C for the pulsed laser deposition (PLD) technique. This indicates that the BFO film grown by the rf sputtering technique undergoes less thermal expansion/contraction history than that by the PLD technique throughout the growth procedure. This could be a potential benefit of the rf sputtering technique over the PLD technique to grow high quality BFO films. The cross-sectional TEM samples were prepared by the focused ion beam technique, FEI Nova 600, with a Ga ion beam. An ~1 μm-thick Pt thin film was deposited on the surface of the sample to prevent possible surface damage and re-deposition during the milling process. The Ga ion beam energy gradually decreased from 30 to 1 keV to minimize ion beam induced damage. For bright-field (BF) imaging, selected area electron diffraction (SAED), atomic resolution high angle annular dark field (HAADF)–scanning TEM (STEM) analysis, and a 200 kV JEOL JEM-ARM200F TEM equipped with probe and image aberration (C_s) correctors and a CCD camera were used. X-ray reciprocal space mapping (XRSM) was performed using a Rigaku SmartLab diffractometer with Cu$K\alpha$ radiation.

Note that the hexagonal notation is used for BFO throughout this work for the accurate evaluation of lattice mismatch between BFO and the LSAT substrate.[26,27]

RESULTS AND DISCUSSION

Figure 1(a) is a cross-sectional BF TEM image of the BFO film grown on the LSAT substrate. It shows an ~150 nm BFO layer grown on the LSAT substrate with the lattice imperfection-induced contrasts at the BFO/LSAT interface as denoted by arrows. Note that the Pt layer is deposited on top of the BFO film owing to the aforementioned reason. In order to acquire crystal structure information within the BFO layer and its epitaxial relation with the LSAT substrate, selected area electron diffraction (SAED) patterns for the BFO layer only, i.e., from circle 1, and the BFO layer with LSAT, i.e., from circle 2, were obtained by using a ~150 nm aperture as shown in Figs. 1(b) and 1(c), respectively. In addition, a SAED pattern for the LSAT substrate was also acquired from an area away from the BFO/LSAT interface with the same size aperture to use as a reference for crystal orientation and camera length calibration as shown in Fig. 1(d). For precise SAED pattern analyses, structure factor, F_{hkl},

$$F_{hkl} = \sum_n f_n \exp[2\pi i(hx_n + ky_n + lz_n)],$$

where hkl represents a specific Bragg's reflection and f_n is the atomic scattering factor for atom n at fractional coordinates (x_n, y_n, z_n), was calculated by using the crystallographic data, i.e., space group, lattice parameter, and basis atom locations, of unstrained rhombohedral BFO, i.e., space group of *R3c*,[28] and unstrained cubic LSATs, i.e., space groups of $Fm\bar{3}m$[29] and $Pm\bar{3}m$[29] materials. The
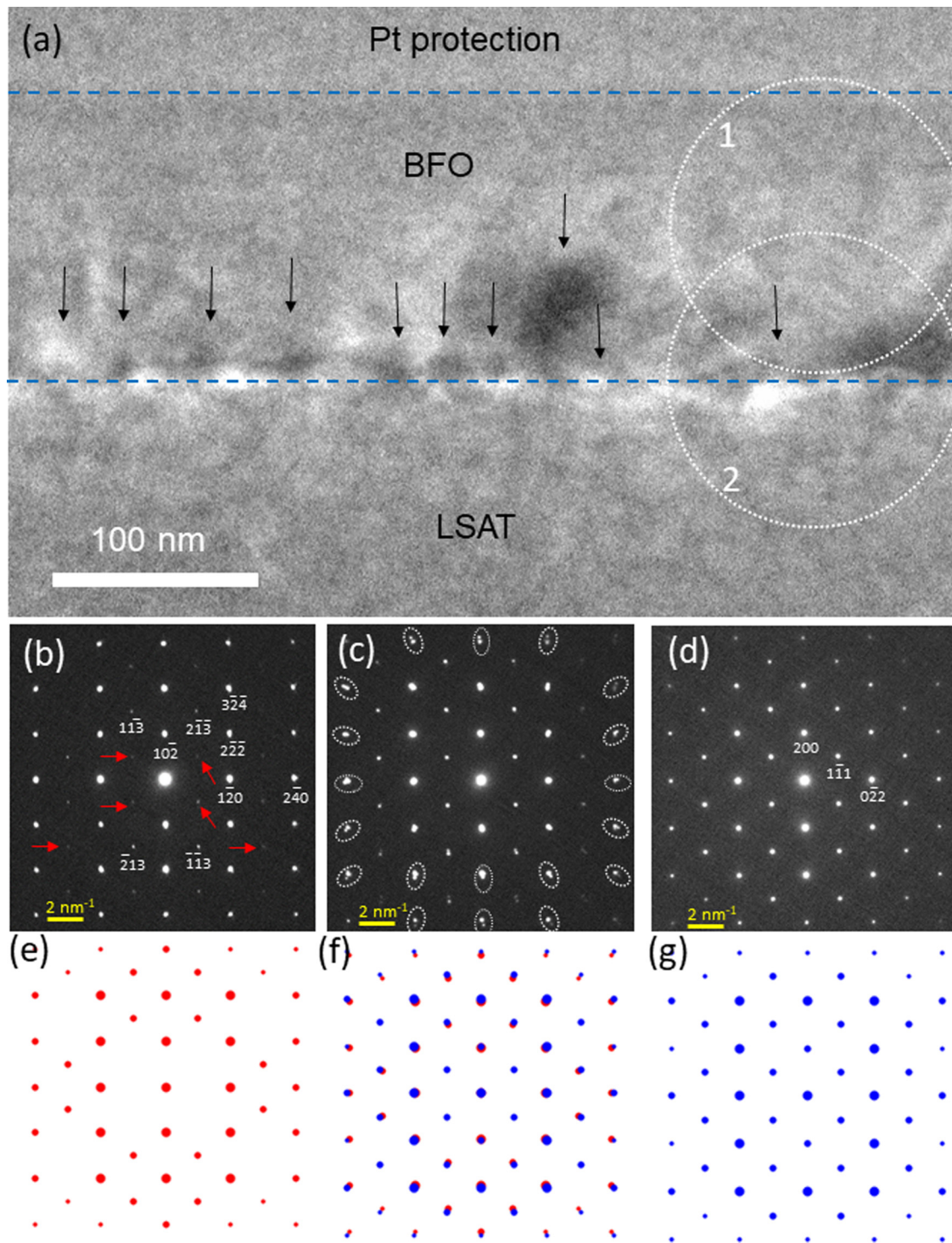
FIG. 1. (a) A cross-sectional BF TEM image of the BFO layer grown on the LSAT substrate along the $[011]_{LSAT}$ zone axis. Lattice imperfection-induced contrasts are denoted by arrows. The SAED patterns from BFO only, BFO plus LSAT, and LSAT only are shown as (b), (c), and (d), respectively. The corresponding structure factor calculation of each SAED pattern are shown as (e), (f), and (g). Circles 1 and 2 indicate the area where the SAED patterns are acquired.

corresponding structure factor calculation results are shown in Figs. 1(e)–1(g). Note that Fig. 1(b) matches the [211] zone axis of rhombohedral BFO, i.e., Fig. 1(e), immaculately by clearly showing rhombohedral signature Bragg's reflections, i.e., such as $2\overline{1}\overline{3}$, $11\overline{3}$, $\overline{2}1\overline{3}$, and $\overline{11}3$, which have been discussed elsewhere.[18–20,23,26,27] Red arrows in Fig. 1(b) indicate the reflections resulting from double diffraction.[30,31] Thus, the BFO crystal structure is unambiguously confirmed rhombohedral with the space group $R3c$. The structure factor calculation for the LSAT materials reveals that the SAED pattern in Fig. 1(d) matches the [011] zone axis of the cubic LSAT with the space group $Fm\overline{3}m$ only, as shown in Fig. 1(g). This confirms the crystal structure of the LSAT substrate as cubic with the space group $Fm\overline{3}m$.[29] Note that another SAED pattern is obtained from the area including both BFO and LSAT as shown in Fig. 1(c). This provides information about the BFO lattice strain status against the LSAT substrate. It is readily noticed that the high index Bragg's reflections from BFO and LSAT split radially with respect to the direct beam located at the center as denoted by the dotted circles. The same characteristic is found in the corresponding Bragg's reflections of the structure factor calculation in Fig. 1(f), obtained by *unstrained* BFO (in red) and *unstrained* LSAT (in blue). This suggests that most of the lattice strain caused by the lattice mismatch between BFO and LSAT is not stored in BFO but rather relaxed by the formation of lattice imperfections. A similar result of the lattice mismatch *not* causing lattice strain was previously reported in the case of epitaxial BFO grown on a single crystal $YAlO_3$ substrate.[27]

In order to provide a direct evidence of lattice strain relaxation in the BFO layer, a HAADF-STEM image was acquired at the BFO/LSAT interface as shown in Fig. 2. One can readily find the missing $(1\overline{2}0)_{BFO}$ lattice planes, i.e., misfit dislocations, against the corresponding $(0\overline{2}2)_{LSAT}$ lattice plane as denoted by red arrows. This clearly indicates that most of the misfit strain is relaxed rather than stored as elastic energy in the BFO layer.
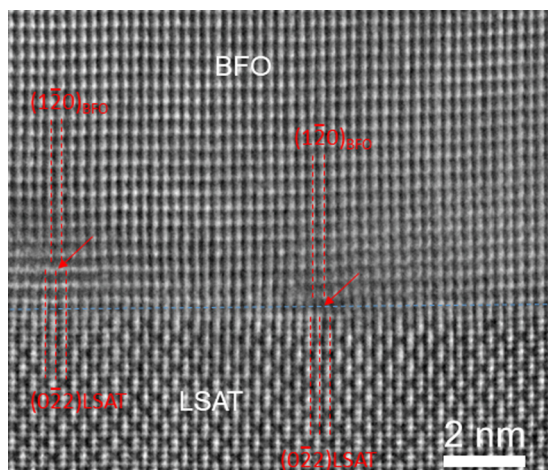
In order to add more insight into the reason for the relaxed lattice strain, the possibility of domain structures within the entire BFO layer was investigated by using the XRSM technique as shown in Fig. 3. Figure 3(a) shows the X-ray intensity profile along Q_z, i.e., along $[100]_{LSAT}$, and Q_x, i.e., along $[0\overline{1}1]_{LSAT}$, orientations. Note that high index BFO reflections show the signs of split (see, for example, the ones denoted by a square and a circle in red). This indicates that the BFO layer consists of two domains having different crystal orientations. In order to find the orientation relation between two domains, i.e., BFO I and BFO II, structure factor calculation is performed by using BFO I (in red) and II (in blue) as shown in Fig. 3(b). The result shows that the $(3\overline{2}4)$ reflection of BFO I and the $(10\overline{8})$ reflection of BFO II are responsible for the

FIG. 2. A cross-sectional HAADF-STEM image at the BFO/LSAT interface along the $[011]_{LSAT}$ zone axis. It clearly shows two misfit dislocations near the BFO/LSAT interface as denoted by the red arrows.
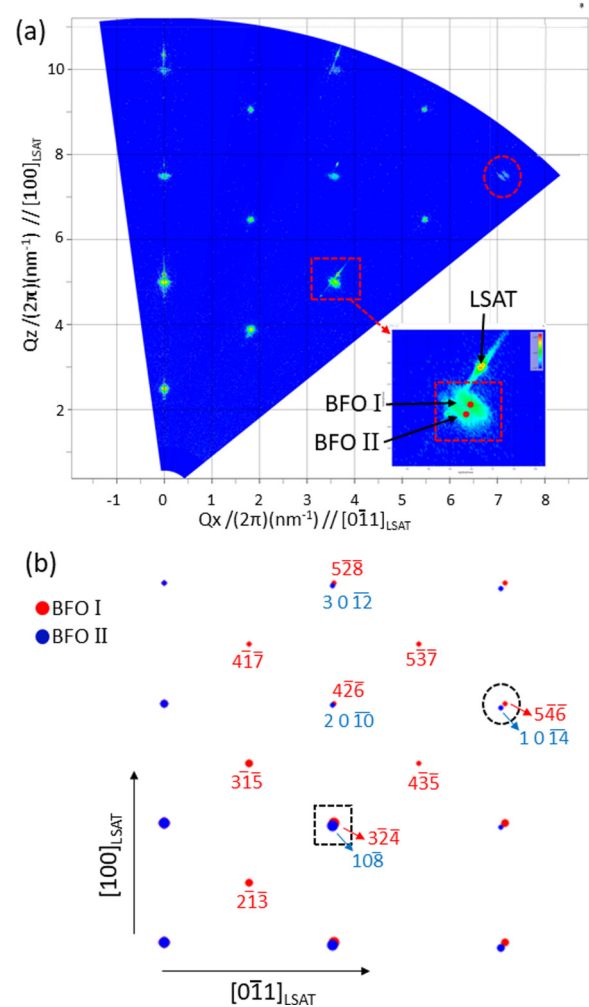
FIG. 3. (a) XRSM data that show X-ray intensity with the two orthogonal orientations, i.e., Q_z that is parallel to $[100]_{LSAT}$ and Q_x that is parallel to $[0\overline{1}1]_{LSAT}$. (b) The corresponding structure factor calculation demonstrating the two BFO domains, i.e., BFO I and BFO II.

split found in the square in Fig. 3(a). In addition, another clear split denoted with a circle in Fig. 3(a) resulted from the $(5\bar{4}6)$ reflection of BFO I and the $(10\bar{1}4)$ reflection of BFO II. In order to further confirm the orientation relation between the two BFO domains, another reciprocal space mapping was performed with an X-ray incident orientation that was rotated 45° around the surface normal orientation as shown in Fig. 4(a). Note that while Q_z is along the $[100]_{LSAT}$ orientation, i.e., the same as in Fig. 3(a), Q_x is now along the $[0\bar{1}0]_{LSAT}$ orientation, i.e., 45° off Q_x used in Fig. 3(a) with respect to the $[100]_{LSAT}$ orientation. The split in high index Bragg's reflections is also detected as can be seen, for example, in the dotted circle. Structure factor calculation shown in Fig. 4(b) indicates that the split is responsible for the $(4\bar{2}0)$ reflection of BFO I and the $(2\bar{2}8)$ reflection of BFO II.

Since X-ray diffraction provides exceptional precision in measuring the lattice plane distance, let us compare the measured lattice plane distances and the corresponding distances calculated
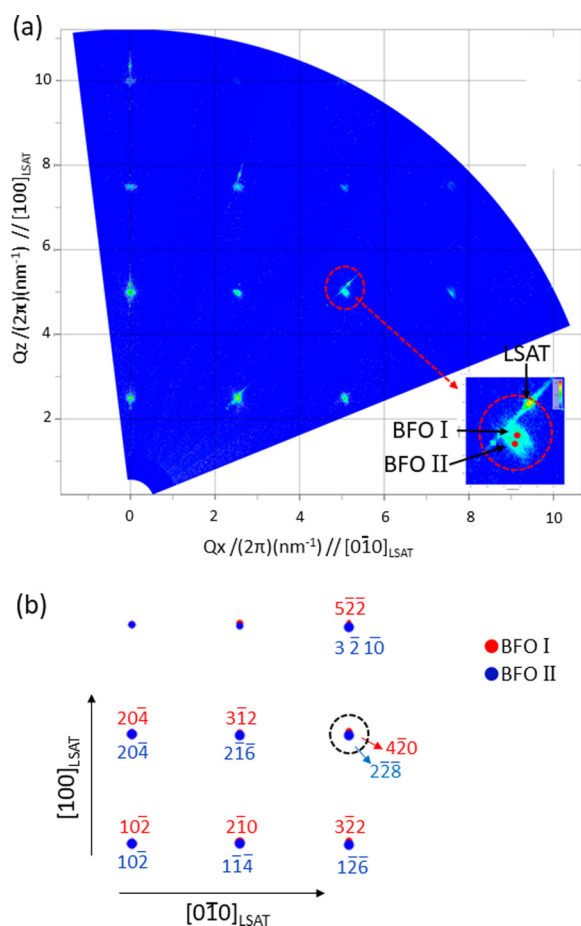
based on the unstrained BFO[28] to investigate the volume-averaged lattice strain status in the BFO layer. The result summarized in Table I clearly shows that the XRSM measurement is consistent with the theoretical calculation, indicating no lattice strain is applied either in BFO I or BFO II domains. This is consistent with the TEM data discussed in Figs 1 and 2.

In order to quantify the lattice misfit between the two BFO domains, i.e., BFO I and BFO II, and the LSAT substrate, epitaxial relations are derived based on the structure factor calculation shown in Figs. 1, 3, and 4 as follows:

$$[211]_{BFO\ I}//[011]_{LSAT}; \quad (10\bar{2})_{BFO\ I}//(100)_{LSAT}, \quad (1)$$

$$[0\bar{1}0]_{BFO\ II}//[011]_{LSAT}; \quad (10\bar{2})_{BFO\ II}//(100)_{LSAT}. \quad (2)$$

Figure 5 shows the atomistic models of (a) BFO I with LSAT and (b) BFO II with LSAT, respectively. The lattice mismatch between BFO I and LSAT was calculated as ~2.2% by comparing in-plane lattice distances, i.e., $(1\bar{2}0)_{BFO\ I} = 0.279$ nm and $(0\bar{2}2)_{LSAT} = 0.273$ nm as shown in Fig. 5(a). The lattice mismatch between BFO II and LSAT was also calculated as ~2.8% by comparing in-plane lattice distances, i.e., $(\bar{1}0\bar{4})_{BFO\ II} = 0.281$ nm and $(0\bar{2}2)_{LSAT} = 0.273$ nm as shown in Fig. 5(b). Given that ~0.35% tensile lattice misfit with the $KTaO_3$ substrate[26] and ~1.0% compressive lattice misfit with the $La_{0.6}Sr_{0.4}MnO_3$ substrate[27] are proven to be stored as lattice strain in BFO epitaxial layers with no sign of misfit dislocations previously, ~2.2% and ~2.8% of compressive lattice misfits found in this study with the LSAT substrate are thought to be too large to be stored as lattice strain in the BFO layer. In fact, 6.8% of compressive lattice misfit is already found too large to be stored as lattice strain in the case of the $YAlO_3$ substrate.[27]

It is worth noting that the orientation relationship between the two BFO domains, i.e., BFO I and BFO II, shows that BFO I and BFO II are rotated around the $(10\bar{2})$ plane normal axis because $(10\bar{2})$ lattice planes in each domain run parallel as shown in the orientation relations (1) and (2). Since the angle between $[211]_{BFO\ I}$ and $[0\bar{1}0]_{BFO\ II}$ is calculated as 90°, it becomes clear that the two domains are 90° off each other around the $(10\bar{2})$ plane normal axis.

Now, let us turn our attention to how the epitaxial relations found above, i.e., (1) and (2), are compared with ferroelectric polarization orientations. Figure 6 shows three dimensional schematics in which ferroelectric polarization orientations, i.e., [001] of domains I (a) and II (b) are shown. Note that (1) the surfaces of

TABLE I. Comparison of the measure lattice plane distances of both BFO I and BFO II with the calculated ones of unstrained BFO.

Lattice planes	XRSM measurement (nm)		Calculation[27] (nm)
	Domain I	Domain II	
$3\bar{2}4$	0.1622		0.161
$5\bar{4}6$	0.0961		0.096
$10\bar{8}$		0.1637	0.163
$10\bar{1}4$		0.0972	0.097

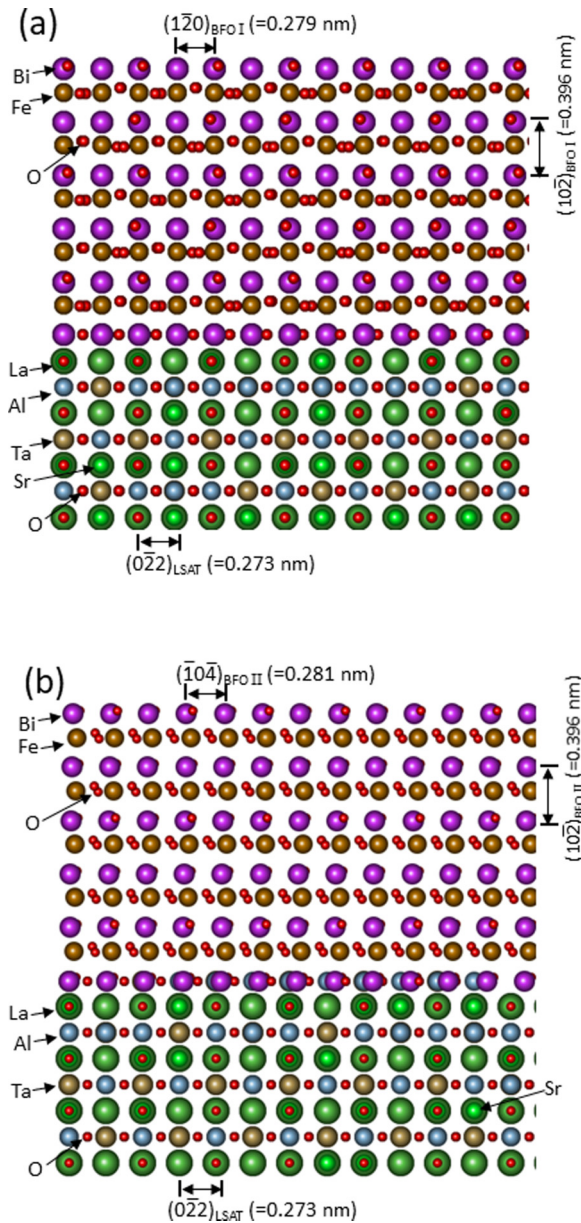**FIG. 5.** Atomistic models that show (a) LSAT/BFO I and (b) LSAT/ BFO II lattice mismatches along the [011]$_{LSAT}$ orientation.
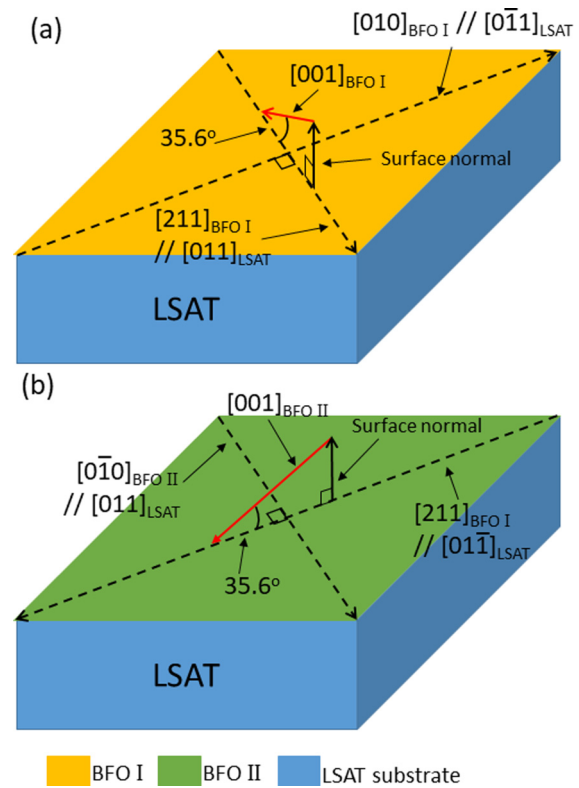

FIG. 6. Three dimensional schematics that show ferroelectric polarization orientations of (a) BFO I and (b) BFO II.

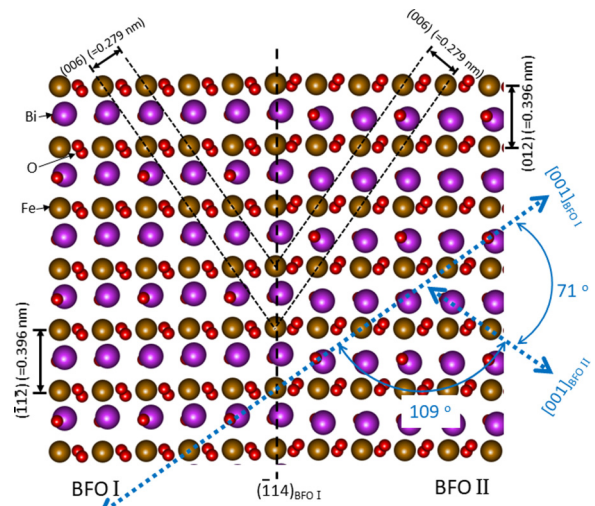**FIG. 7.** An atomistic model that shows the ferroelectric orientation relation, i.e., the angle between [001]$_{BFO\ I}$ and [001]$_{BFO\ II}$. Note that the ($\bar{1}$14)$_{BFO\ I}$ interface is assumed for convenience.

BFO I and BFO II grown on top of the (100) LSAT surface are (10$\bar{2}$), and (2) the orientation of the diagonal lines denoted on the surfaces of BFO films corresponds to ⟨011⟩$_{LSAT}$. The angles between the BFO film surface and [001]$_{BFO\ I}$ are calculated as 35.6° for both domains as denoted in Figs. 6(a) and 6(b). In addition, it is also found that the in-plane components of both ferroelectric polarization axes run parallel to diagonal directions, i.e.,⟨011⟩$_{LSAT}$. While this is interesting, it should be pointed out that this result is

based solely on crystallographic data. Thus, we believe further study with direct measurement of ferroelectric polarization is needed to confirm the polarity of each ferroelectric polarization axis.

In order to compare the orientations relation found between BFO I and BFO II with the BFO ferroelectric domain structures reported previously, i.e., 71°, 109°, and 180° domain structures,[32,33] an atomistic model is created by using the orientation relations (1) and (2) as shown in Fig. 7. Note that the zone axis of the model, i.e., projection orientation, is chosen as $[110]_{BFO\ I}$ to show the ferroelectric polarization orientations, i.e., $[001]_{BFO}$, of each domain. Since this zone axis is orthogonal to the ferroelectric polarization axes of both BFOs I and II, the angle between the two ferroelectric polarization axes can be directly measured two dimensionally as depicted in Fig. 7. The interface between BFO I and BFO II in this model is assumed as $(\bar{1}14)_{BFO\ I}$ for convenience. Two possible angles, i.e., 71° and 109° between $[001]_{BFO\ I}$ and $[001]_{BFO\ II}$, are readily noticed depending on the combinations of polarity of the ferroelectric polarization axes in each domain. This indicates that the BFO domain structure found in this study is in agreement with 71° and/or 109° ferroelectric domain structures discussed previously.[32,33] Since the 180° domain structure is purely ferroelectric as opposed to the ferroelastic 71° and 109° domain structures discussed here,[34] further investigation with the direct measurement of the polarity of ferroelectric polarization axis is needed for discussion.

While the domain structure is widely reported in pulsed laser deposition prepared epitaxial BFO films including a co-substituted BFO epitaxial film grown on $CaRuO_3$ coated LSAT,[35] such a domain structure was, interestingly, not found in the ultrahigh vacuum rf sputter grown BFO films reported previously with $LaAlO_3$,[20] $KTaO_3$,[26] and $La_{0.6}Sr_{0.4}MnO_3/SrTiO_3$ substrates[27] where lattice mismatches are stored as biaxial lattice strain in the BFO epitaxial layers. Volume-averaged X-ray diffraction data for those substrates indicate that the BFO epitaxial layers have a mono-domain structure. Given that the domain boundary and dislocation are lattice defects where lattice strain can be relaxed, a defect-free mono-domain structure in BFO is speculated to be required for lattice strain to be preserved in epitaxial BFO. Further study with different substrates with various crystal orientations is necessary to elucidate this point.

CONCLUSIONS

In summary, an epitaxial BFO layer is grown on the LSAT (100) substrate to investigate the lattice misfit effect of LSAT on the BFO overlayer in terms of crystal structure, lattice strain status, and domain structure. TEM and SAED data clearly show that the crystal structure of the BFO layer is the same as unstrained bulk BFO, i.e., space group $R3c$. This is consistent with the misfit dislocations directly observed by atomic resolution HAADF-STEM techniques. Volume-averaged XRSM data indicate that the BFO layer consists of two domains that were rotated 90° along the surface normal orientation. In addition, further investigation with the structure factor calculation suggests that the ferroelectric polarization axes of the two domains are found to be 35.6° with respect to BFO film surface with their in-plane components parallel to the diagonal orientations of the LSAT substrate. An atomistic model

created on the basis of the epitaxial relation found between the two domains confirms that the ferroelectric polarization orientations, i.e., $[001]_{BFO}$, of the two domains are 71° and/or 109° off each other, which is in good agreement with 71° and 109° domain structures discussed previously. The ~2.8% misfit strain found based on the epitaxial relation between BFO and LSAT is suggested to be too large to be stored as lattice strain in BFO.

DATA AVAILABILITY

The data that support the findings of this study are available within the article.

REFERENCES

[1]G. A. Smolenskii and I. E. Chupis, Sov. Phys. Usp. **25**, 475 (1982).

[2]S. V. Kiselev, R. P. Ozerov, and G. S. Zhdanov, Sov. Phys. Dokl. **7**, 742 (1963); available at https://ui.adsabs.harvard.edu/abs/1963SPhD....7..742K/abstract.

[3]J. Wang, J. B. Neaton, H. Zheng, V. Nagarajan, S. B. Ogale, B. Liu, D. Viehland, V. Vaithyanathan, D. G. Schlom, U. V. Waghmare, N. A. Spaldin, K. M. Rabe, M. Wuttig, and R. Ramesh, Science **299**, 1719 (2003).

[4]W. Erenstein, F. D. Morrison, J. Dho, M. G. Blamire, J. F. Scott, and N. D. Mathur, Science **307**, 1203 (2005).

[5]D. Lebeugle, D. Colson, A. Forget, M. Viret, P. Bonville, J. F. Marucco, and S. Fusil, Phys. Rev. B **76**, 024116 (2007).

[6]D. Lebeugle, D. Colson, A. Forget, and M. Viret, Appl. Phys. Lett. **91**, 022907 (2007).

[7]C. Ederer and N. A. Spaldin, Phys. Rev. Lett. **95**, 257601 (2005).

[8]D. G. Schlom, L.-Q. Chen, C. J. Fennie, V. Gopalan, D. A. Muller, X. Pan, R. Ramesh, and R. Uecker, "Elastic strain engineering of ferroic oxides," MRS Bull. **39**, 118 (2014).

[9]D. Ricinschi, K. Y. Yun, and M. Okuyama, J. Phys. Condens. Matter **18**, L97 (2006).

[10]G. Xu, J. Li, and D. Viehland, Appl. Phys. Lett. **89**, 222901 (2006).

[11]H. Béa, B. Dupe, S. Fusil, R. Mattana, E. Jacquet, B. Warot-Fonrose, F. Wilhelm, A. Rogalev, S. Petit, V. Cros, A. Anane, F. Petroff, K. Bouzehouane,

G. Geneste, B. Dkhil, S. Lisenkov, I. Ponomareva, L. Bellaiche, M. Bibes, and A. Barthélémy, Phys. Rev. Lett. **102**, 217603 (2009).

[12]R. J. Zeches, M. D. Rossell, J. X. Zhang, A. J. Hatt, Q. He, C.-H. Yang, A. Kumar, C. H. Wang, A. Melville, C. Adamo, G. Sheng, Y.-H. Chu, J. F. Chu, J. F. Ihlefeld, R. Erni, C. Ederer, V. Gopalan, L. Q. Chen, D. G. Schlom, N. A. Spaldin, L. W. Martin, and R. Ramesh, Science **326**, 977 (2009).

[13]Z. Chen, L. You, C. Huang, Y. Qi, J. Wang, T. Sritharan, and L. Chen, Appl. Phys. Lett. **96**, 252903 (2010).

[14]H. M. Christen, J. H. Nam, H. S. Kim, A. J. Hatt, and N. A. Spaldin, Phys. Rev. B **83**, 144107 (2011).

[15]Z. Chen, Z. L. Luo, C. W. Huang, Y. J. Qi, P. Yang, L. You, C. S. Hu, T. Wu, J. L. Wang, C. Gao, T. Sritharan, and L. Chen, Adv. Funct. Mater. **21**, 133 (2011).

[16]J. C. Yang, Q. He, S. J. Suresha, C. Y. Kuo, C. Y. Peng, R. C. Haislmaier, M. A. Motyka, G. Sheng, C. Adamo, H. J. Lin, Z. Hu, L. Chang, L. H. Tjeng, E. Arenholz, N. J. Podraza, M. Bernhagen, R. Uecker, D. G. Schlom, V. Gopalan, L. Q. Chen, C. T. Chen, R. Ramesh, and Y. H. Chu, Phys. Rev. Lett. **109**, 247606 (2012).

[17]Z. Chen, Y. Qi, L. You, P. Yang, C. W. Huang, J. Wang, T. Sritharan, and L. Chen, Phys. Rev. B **88**, 054114 (2013).

[18]I.-T. Bae and H. Naganuma, Appl. Phys. Express **8**, 031501 (2015).

[19]I.-T. Bae, H. Naganuma, T. Ichinose, and K. Sato, Phys. Rev. B **93**, 064115 (2016).

[20]I.-T. Bae, A. Kovács, H. J. Zhao, J. Iniguez, S. Yasui, T. Ichinose, and H. Naganuma, Sci. Rep. **7**, 46498 (2017).

[21]O. Diéguez, O. E. González-Vázquez, A. C. Wojdel, and J. Íñiguez, Phys. Rev. B **83**, 094105 (2011).

[22]D. Sando, B. Xu, L. Bellaiche, and V. Nagarajan, Appl. Phys. Rev. **3**, 011106 (2016).

[23]I.-T. Bae, T. Ichinose, S. Yasui, A. Kovács, H. J. Zhao, J. Íñiguez, and H. Naganuma, Jpn. J. Appl. Phys. **57**, 0902A5 (2018).

[24]S. C. Tidrow, A. Tauber, W. D. Wilber, R. T. Lareau, C. D. Brandle, G. W. Berkstresser, A. J. Ven Graitis, D. M. Potrepka, J. I. Budnick, and J. Z. Wu, IEEE Tans. Appl. Supercond. **7**, 1766 (1997).

[25]C. L. Canedy, S. Aggarwal, H. Li, T. Venkatesan, R. Ramesh, F. W. Van Keuls, R. R. Romanofsky, and F. A. Miranda, Appl. Phys. Lett. **77**, 1523 (2000).

[26]I.-T. Bae, T. Ichinose, M.-G. Han, Y. Zhu, S. Yasui, and H. Naganuma, Sci. Rep. **8**, 893 (2018).

[27]I.-T. Bae, S. Yasui, T. Ichinose, M. Itoh, T. Shiraish, T. Kiguchi, and H. Naganuma, Sci. Rep. **9**, 6715 (2019).

[28]A. Reyes, C. de la Vega, M. E. Fuentes, and L. Fuentes, J. Eur. Ceram. Soc. **27**, 3709 (2007).

[29]H. Li, L. Salamanca-Riba, R. Ramesh, and J. H. Scott, J. Mater. Res. **18**, 1698 (2003).

[30]P. Hirsch, A. Howie, R. B. Nicholson, D. W. Pashley, and M. Whelan, *Electron Microscopy of Thin Crystals* (Krieger Pub. Co., New York, 1977), Chap. 5.5.

[31]D. B. Williams and C. B. Carter, *Transmission Electron Microscopy* (Plenum, New York, 1996), Chap. 18.

[32]H. W. Jang, D. Ortiz, S.-H. Baek, C. M. Folkman, R. R. Das, P. Shafer, Y. Chen, C. T. Nelson, X. Q. Pan, R. Ramesh, and C.-B. Eom, Adv. Mater. **21**, 817 (2009).

[33]G. Catalan and J. F. Scott, Adv. Mater. **21**, 2463 (2009).

[34]J. Sapriel, Phys. Rev. B **12**, 5128 (1975).

[35]D. Y. Wang, N. Y. Chan, R. K. Zheng, C. Kong, D. M. Lin, J. Y. Dai, H. L. W. Chan, and S. Li, J. Appl. Phys. **109**, 114105 (2011).